


**Fermilab**

# IV and CV curves for Irradiated Prototype BTeV Silicon Pixel Sensors

Maria R. Coluccia, J.A. Appel, G. Chiodini, D.C. Christian, S.W. Kwan, G. Sellberg, and L. Uplegger

**Abstract**—We present IV and CV curves for irradiated prototype  $n^+/n/p^+$  silicon pixel sensors, intended for use in the BTeV experiment at Fermilab. We tested pixel sensors from various vendors and with two pixel isolation layouts: p-stop and p-spray. Results are based on exposure with 200MeV protons up to  $6 \times 10^{14}$  protons/cm<sup>2</sup>.

## I. INTRODUCTION

High energy and nuclear physics experiments need tracking devices with increasing spatial precision and readout speed in the face of ever higher track densities and increased radiation. We report here on the tolerance of hybrid silicon pixel components intended for use in BTeV [1], a heavy quark experiment at Fermi National Accelerator Laboratory (Illinois, USA). The BTeV experiment plans to run at the Tevatron Collider. It is designed to cover the “forward” region of the proton-antiproton interaction point running at a luminosity of  $2 \times 10^{32}$  cm<sup>-2</sup>s<sup>-1</sup>. The experiment will employ a silicon pixel vertex detector to provide high precision space points for an on-line lowest-level trigger based on track impact parameters [2].

The baseline BTeV silicon pixel detector has rectangular 50 μm x 400 μm pixel elements. It consists of a regular array of 30 “stations” of “planar” pixel detectors distributed along the IR (Interaction Region). Each station contains one plane with the narrow pixel dimension vertical, and one with the narrow dimension horizontal. The stations are split in order to move the sensors away from the beam during the setup and other unstable beam conditions. See Fig. 1 for details.

The vertex detector contains nearly 22 million rectangular pixels. A dedicated electronics cell reads out each sensor element, and a “bump bond” connects the sensor pixel to the readout cell. The basic building block of the detector is a hybrid assembly consisting of a sensor, a number of readout chips (FPIX2 chip [3] developed at Fermilab), and a flexible printed circuit (a high-density interconnect, HDI), which carries I/O signals and power. The sensors are variously sized to accept variable numbers of readout chips to make the required half-plane shape. Each readout chip is “flip-chip” mated to 22 columns of 128 rows of pixels on the sensors, corresponding to 2,816 active channels per readout chip.

Each readout chip covers an active area approximately 0.64 cm x 0.92 cm. To avoid any dead space between adjoining readout chips, the pixels on the sensors corresponding to the edge of the readout chip (first and last column) are extended to 600 μm length.

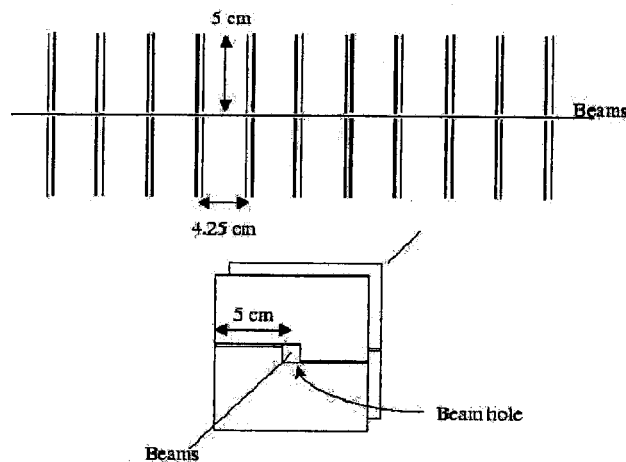


Fig. 1. Schematic drawing of part of the BTeV vertex detector.

Each station has a small square hole of  $\pm 6$  mm x  $\pm 6$  mm for the beam to pass through. At such small distance from the colliding beams, the pixel detectors will be exposed to a significant level of irradiation. At the full luminosity at which we plan to operate, the innermost pixel detector will receive an equivalent fluence of  $\sim 10^{14}$  minimum ionizing particles/cm<sup>2</sup>/year. This will lead to radiation damage of the silicon pixel sensors.

Due to this harsh environment, the performance of the BTeV pixel sensors will be degraded with time. The degradation includes an increase of both leakage current and full depletion voltage, and a decrease in charge collection efficiency. These are problems that need to be address by all the next generation hadron collider experiments. As a result, there is a worldwide effort to address these technical challenges. Solutions include the design of multi guard ring structures to avoid avalanche breakdown along the edge, low resistivity silicon substrates to delay type inversion, and oxygenated wafers to reduce the effects of radiation-induced defects in the silicon lattice.

Manuscript received July 16, 2002. This work was supported in part by the U.S. Department of Energy.

The first six authors are with Fermi National Accelerator Laboratory, P.O. Box 500 Batavia, IL 60510 USA.

The last author is with Istituto Nazionale di Fisica Nucleare, Milano, via Celoria 16-20133, Italy.

## II. THE SENSOR CONCEPT

In order to increase the lifetime of the silicon sensors, operation with partial depletion has to be considered. For this reason, the BTeV pixel sensors have  $n^+/n/p^+$  configuration. After bulk type inversion, the depleted region grows from the  $n^+$  side of the junction and the sensor can operate partially depleted. Such operation might be necessary if the full depletion voltage becomes excessively large after substrate type inversion caused by the high irradiation. However, for  $n^+/n$  devices, it is necessary to provide explicit electrical isolation between neighboring  $n^+$  electrodes. Without isolation, the accumulation layer induced by oxide charge buildup would short the individual  $n^+$  electrodes. Various isolation techniques have been developed for silicon pixel sensors. Here we explore two techniques: p-stop and moderated p-spray.

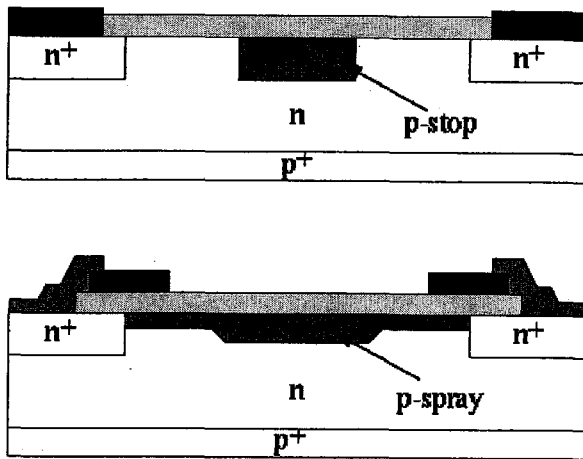


Fig. 2. Schematic views of the implants in the p-stop (top) and moderated p-spray (bottom) electrode isolation methods.

In the case of the p-stop isolation technique, a high dose p-implant surrounds each  $n^+$ -type region. Here we tested pixel sensors having two different layouts of p-stop [4] electrode isolation: individual and common p-stops. For the individual p-stop there is a p-implant ring (atoll) around each pixel. For the common p-stop, there is a continuous p-implant between pixel columns and rows. The p-spray [5] isolation technique was developed by the ATLAS collaboration and consists of a medium dose p-implant that is applied to the entire n-side and is overcompensated by the high dose  $n^+$  pixel implants. To increase radiation hardness and also to increase the breakdown voltage before irradiation, a “grading” of p-spray implantation (moderated p-spray) [6] is used. This technique leads to a step in the effective p-spray dose along the gap between two  $n^+$ -implants. In the middle of the gap, the normal p-spray dose is reached. This guarantees the inter-pixel isolation. Near the edges, the p-spray dose is lower in order to minimize the electric field strength in these regions and therefore improve breakdown performance [7]. Fig.2

shows a schematic view of both p-stop and p-spray isolation methods.

In the p-spray technique, a bias grid structure was implemented in order to apply the bias voltage to all pixels simultaneously prior to bump bonding. This structure is very important for quality control during mass production and is very useful for testing the sensors before and after irradiation in the development phase. Moreover, in case of missing bonds, this bias grid acts as a safety feature during operation, maintaining unconnected  $n^+$  electrode potentials closer to ground. The bias grid connects every pixel via an equally sized punch-through gap applying the same potential to every individual pixel. For the p-stop design it is not possible to have a bias grid because this would have to cross the p-stop implant.

Finally, a controlled potential drop toward the cut edge on the p-side is achieved by a multiple guard ring structure, allowed by the double-sided processing of  $n^+n$  sensors. These structures maintain the p edges of the sensors at the same potential as the  $n^+$ -side, which sits at the virtual ground potential of the readout-chip.

## III. DEVICES UNDER TEST

We have tested sensors from three vendors: the p-stop sensors are from SINTEF Electronics and Cybernetics (Oslo, Norway), the p-spray sensors are from TESLA (Roznov, Czech Republic) and from CiS (Erfurt, Germany). The base material for the p-stop sensors is low resistivity ( $1.0\text{-}1.5\text{ K}\Omega\text{ cm}$ )  $\langle 100 \rangle$  silicon,  $270\text{ }\mu\text{m}$  thick. For the p-spray sensors we have higher resistivity ( $2\text{-}5\text{ K}\Omega\text{ cm}$ )  $\langle 111 \rangle$  silicon,  $250\text{ }\mu\text{m}$  thick. Some of the SINTEF and CiS wafers and the all TESLA wafers have been oxygenated.

We tested two different pixel array sizes for p-stop sensors and one for the p-spray. The first p-stop array (called “test-sized sensor”) contains  $12 \times 92$  cells and all these cells, except for four, are connected together. This structure was designed to study the behavior of a single cell. The second array (called “FPIX1-sized sensors”), both for p-stop and p-spray, contains  $18 \times 160$  cells and it is designed to be read out by a single FPIX1 chip [3] that is the first complete high speed digital pixel readout architecture implementation before the development of the final FPIX2 chip. As mentioned above for the p-spray arrays, a bias grid is implemented. In the p-stop array, there is no bias grid and unlike the test-sized sensors, in this case no cells are connected together.

We have four different guard ring structures on the tested devices. We have 16 guard rings for the p-spray sensors, 10 and 18 guard rings for the p-stop test-sized sensors, and 11 guard rings for the FPIX1-sized p-stop sensors. For the structures with 11, 16, and 18 guard rings [8] the design is similar to the one implemented in the ATLAS prototype I design [9]. Each ring has a p-implant  $10\text{ }\mu\text{m}$  wide and the pitch increases from  $20\text{ }\mu\text{m}$  for the innermost ring to  $50\text{ }\mu\text{m}$  near the edge of the detector. In addition, there is a metal field plate that overhangs the p-implant and extends inwards by

half the gap width towards the active area [10]. In the case of 10 guard rings, every ring has 15  $\mu\text{m}$   $\text{p}^+$  implantation, 23  $\mu\text{m}$  of metalization (that overlaps the  $\text{p}^+$  implant by 4  $\mu\text{m}$  on both sides) and 11  $\mu\text{m}$  of passivation opening [11]-[12]. There is a large  $\text{n}^+$  region (400  $\mu\text{m}$ ) between the last guard ring and the dicing scribe line. Going outwards from bias ring toward the  $\text{n}^+$  region, the gaps among adjacent rings increase from 15  $\mu\text{m}$  to 30  $\mu\text{m}$ .

#### IV. EXPERIMENTAL PROCEDURES

Electrical characterization of the devices was performed with standard techniques (I-V,  $V_{\text{g-ring}}$ -V and C-V curves) before and after irradiation. We used a Keithley 237 as power supply and current monitor, and both QTech 7600 and HP4274A LRC meters for the C-V measurements.

All the measurements were performed using a probe station placed in a dark box in a clean room. Continuous monitoring of temperature and humidity were performed, and all the measurements reported were done at 0 % relative humidity, achieved by flowing dry nitrogen in the dark box. In order to investigate the stability of the electrical characteristics, several measurements were performed in various humidity conditions (ranging from 0 % to 40 %), but no significant difference was detected.

The measurements were performed with the p-side (sensor back-plane) biased through one probe, the guard ring floating and the n-side grounded through the support chuck. In order to ground all the cells in the p-stop sensors, a conductive rubber was placed on the probe station chuck. The idea is that the irregular surface of the rubber material should guarantee that all pixels are in good electrical contact with the rubber. This is also due in part to the light pressure on the p-side applied by the probe.

We measured the leakage current and the capacitance for the whole sensor without considering any correction for the contribution from the guard ring region. We performed some measurements before irradiation, biasing the innermost guard ring together with the p-side. However, we found that the contribution from the guard ring region was negligible before irradiation.

Several single devices were characterized before irradiation and some of these also after irradiation. The proton irradiation took place at the Indiana University Cyclotron Facility (IUCF) with a 200 MeV proton beam. The displacement damage cross section for 200 MeV protons (90.5 MeVmb) [13] is almost exactly the same as the value conventionally assigned to 1 MeV neutrons (95 MeVmb) [14] so we quote our results as a function of proton fluence rather than 1 MeV neutron equivalent fluence. The beam profile was measured by exposing a sensitive film. The beam spot, defined by the circular area where the flux is within 90 % of the central value, had a diameter of 1.5 cm, comfortably larger than the sensor size (the FPIX1-sized sensor is  $\sim 1 \text{ cm} \times$

1 cm). Before the exposure, the absolute fluence was measured with a Faraday cup; during the exposure the relative fluence was determined with a Secondary Electron Emission Monitor.

We used a PC board with a big opening in the middle (4 inch  $\times$  4 inch) where we placed the sensors with simple cardboard supports. The irradiation was done in air at room temperature and took no more than six hours. The exposures with multiple boards were done placing the boards about 2 cm behind each other and with the pixel side facing the beam. Mechanically, the boards were kept in position by an open aluminum frame. A maximum of six boards were exposed each time, and therefore the beam energy degradation was negligible. After irradiation, the tested devices were kept at minus 15  $^{\circ}\text{C}$  in order to freeze any beneficial and/or reverse annealing process.

The measurements after irradiation were performed in a condition in which the plateau of the beneficial annealing has not been reached. We are interested in investigating the behavior of the sensors in an environment that is as close as possible to the real experiment. The operational temperature of the vertex detector in BTeV will be between  $-5^{\circ}\text{C}$  and  $-10^{\circ}\text{C}$  and therefore the pixel sensors will not profit from beneficial annealing. For this reason, we decided to store the irradiated sensors at low temperature just after irradiation. The measurements at room temperature took no more than a few hours.

Typically, measurements were made thirty days after irradiation.

#### V. RESULT AND DISCUSSION

##### A. P-Stop Sensor Performance

We tested several test-sized and FPIX1-sized sensors before and after irradiation. Fig. 3 shows the typical I-V curves for both devices before irradiation. The test-sized sensors have very good performance, high breakdown voltage ( $> 500 \text{ V}$ ) and small leakage current ( $\sim 10 \text{ nA/cm}^2$  after depletion). The FPIX1-sized sensors, although the current is also small, present an earlier breakdown voltage (typically just above 300V). The same results were found for all the sensors that were tested.

As pointed out in the previous section, the test-sized sensors are all connected together. So in this case no ground problems arise. For the FPIX1-sized sensors, we have recently investigated in more detail the ground problem in order to understand the cause of the difference in breakdown voltage performance. We observed that the performance of the FPIX1-sized sensors improves considerably after bump bonding to a readout chip. We tested 5 sensors that were bump bonded to a readout chip. Furthermore, we also tested three sensors with indium bumps deposited on the  $\text{n}^+$  side that were then glued with conducting silver epoxy to a piece of silicon in order to mimic the presence of the readout chip. Apart from one sensor bonded to a chip that has a breakdown voltage around 300V, all the others show a breakdown

voltage higher than 500V. Unfortunately, the only sensor that has an early onset of the breakdown is also the one that we reported in our previous paper leading to a misunderstanding of our result [15]. Fig. 4 shows the I-V curves for an FPIX1-sized sensor before the bump bonding to the electronics and after the bump bonding with the readout chip. We conclude that even though the conductive rubber was chosen in order to allow all the cells to be grounded simultaneously, the irregular surface does not guarantee that all the single cell pads are grounded properly. This is a problem that we need to consider before choosing the isolation technology for production because we need obviously to test the bare sensors before bonding for quality control of the sensors. There is a problem with implementing such a feature for the p-stop design.

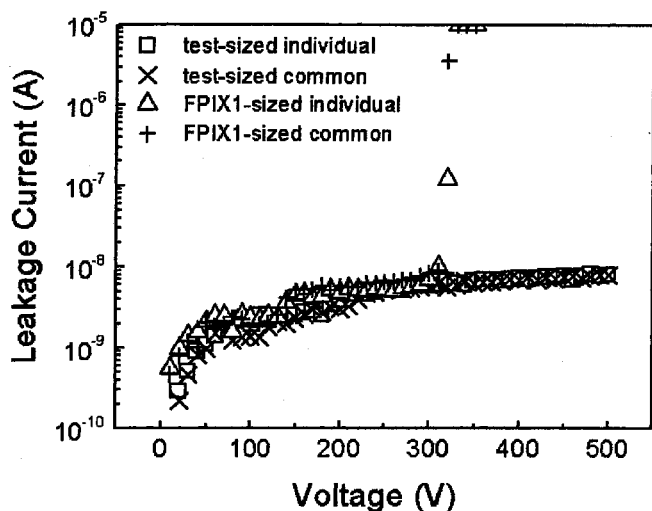


Fig. 3. I-V characteristics for un-irradiated p-stop pixel sensors.

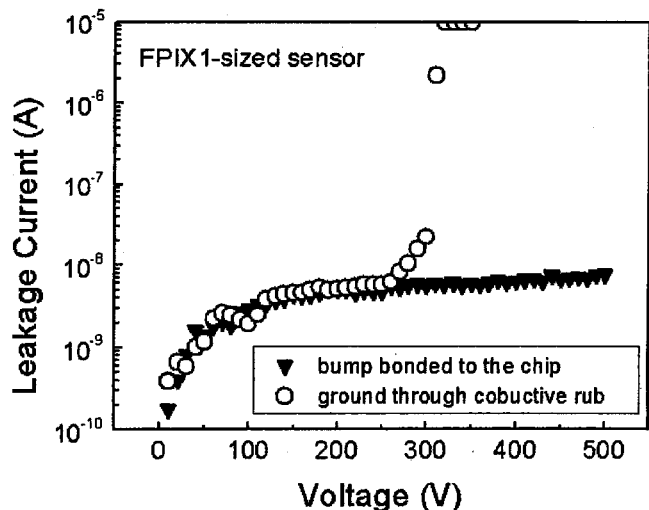


Fig. 4. I-V characteristics for a p-stop FPIX1-sized sensor before and after bump bonding to the readout chip.

Several test-sized and FPIX1-sized sensors were irradiated up to  $6 \times 10^{14} \text{ p/cm}^2$ . Figure 5 shows the IV characteristics

for a test-sized sensor irradiated up to  $1.5 \times 10^{14} \text{ p/cm}^2$ . The leakage current after irradiation increases by several orders of magnitude. However, operating at lower temperature can alleviate this problem. The measurements shown in Fig. 5 were done at  $23^\circ\text{C}$ . We investigated the variation of the leakage current with the temperature in previous work and, as expected, we observed that the current decreases exponentially with temperature [15]. The leakage current after irradiation, as expected, has a nearly linear dependence on fluence [15]. Up to  $6 \times 10^{14} \text{ p/cm}^2$ , the sensors have a breakdown voltage higher than 500 V.

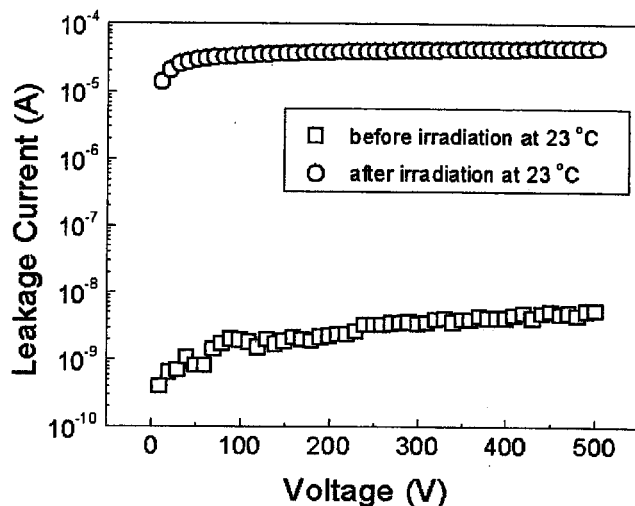


Fig. 5. I-V curves for a common p-stop test-sized sensor before and after irradiation up to  $1.5 \times 10^{14} \text{ p/cm}^2$ . The measurements were performed at room temperature.

In order to investigate the bulk damage induced by radiation, we investigate the variation of the depletion voltage (and therefore the operating voltage) with the proton fluence. It is well known that the depletion voltage depends on the effective doping concentration that changes with the irradiation [16]. The depletion voltage is normally defined as the bias voltage that we need to apply to the sensors in order to have the whole semiconductor bulk completely depleted of free carriers. We extract this value from C-V curves as the intersection point of two fitted straight lines in the  $\log C$ - $\log V$  plot. In Fig. 6 we show a typical example of bulk capacitance versus bias potential for a test-sized common p-stop irradiated up to  $1.2 \times 10^{14} \text{ p/cm}^2$  used to determine the depletion voltage.

Fig. 7 shows the dependence of the full depletion voltage on the proton fluences for the p-stop sensors. We see that the full depletion voltage at  $4 \times 10^{14} \text{ p/cm}^2$  is still very low, lower than the value before the irradiation ( $\sim 210 \text{ V}$ ). This characteristic is due to the low resistivity of the silicon. Even up to a fluence of  $6 \times 10^{14} \text{ p/cm}^2$  (equivalent to 6 years of BTeV running at the nominal luminosity of  $2 \times 10^{32} \text{ cm}^{-2} \text{ sec}^{-1}$ ) the depletion voltage is still low compared to the breakdown voltage ( $> 500 \text{ V}$ ). This result is very

important for the BTeV experiment because we can have fully depleted detectors at acceptable bias voltage.

More results for the p-stop SINTEF sensors can be found in our previous work together with interesting results on oxygenated sensors [15].

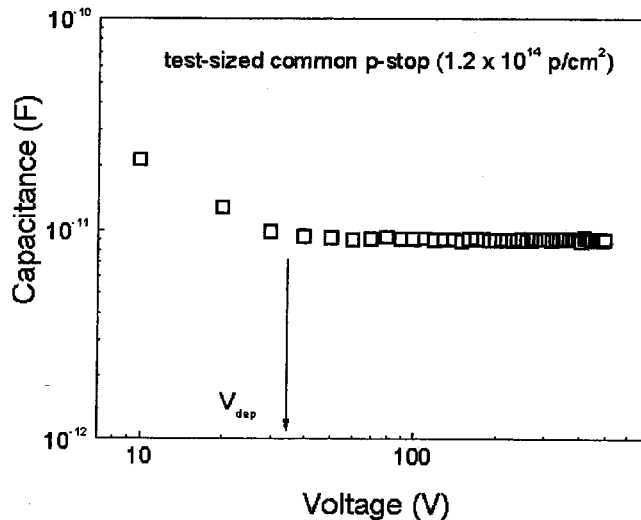


Fig. 6. Example measurement of bulk capacitance versus bias potential, used to determine the depletion voltage of a common p-stop test-sized sensor.

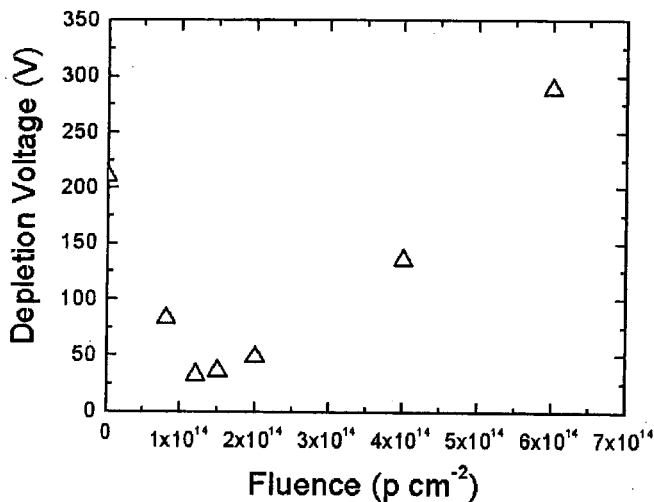


Fig. 7. Depletion voltage as function of proton fluences for p-stop pixel sensors.

### B. P-Spray Sensors Performance

Several wafers from CiS and two from TESLA were tested. Apart from a few sensors that show higher leakage current and low breakdown voltage ( $<300$  V), the typical I-V curves for FPIX1-sized p-spray sensors show a breakdown voltage higher than 500V and a low leakage current (the breakdown voltage is defined as the voltage for which the current increases steeply and is bigger than  $1 \mu\text{A}$ ).

We have irradiated only two of these sensors, one up to  $8 \times 10^{13}$  p/cm<sup>2</sup> and one up to  $1.2 \times 10^{14}$  p/cm<sup>2</sup>. Fig. 8 shows the increase in the leakage current due to the irradiation for the sensor irradiated with the higher dose. Also in this case, the current increases several orders of magnitude.

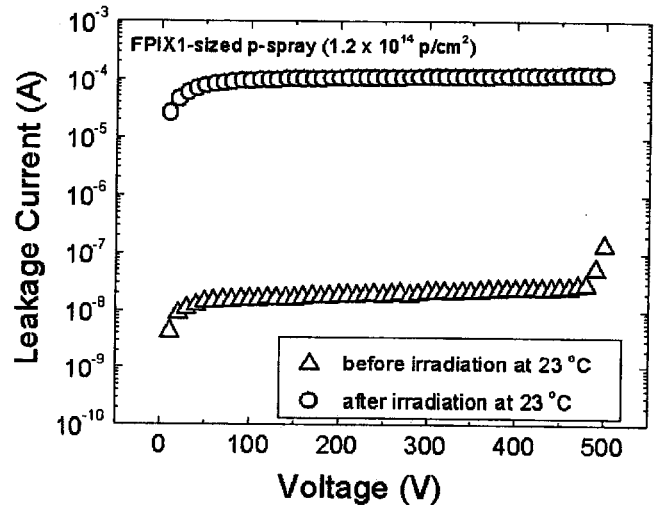


Fig. 8. I-V curves for a FPIX1-sized p-spray sensor before and after irradiation up to  $1.2 \times 10^{14}$  p/cm<sup>2</sup>. The measurements were performed at room temperature.

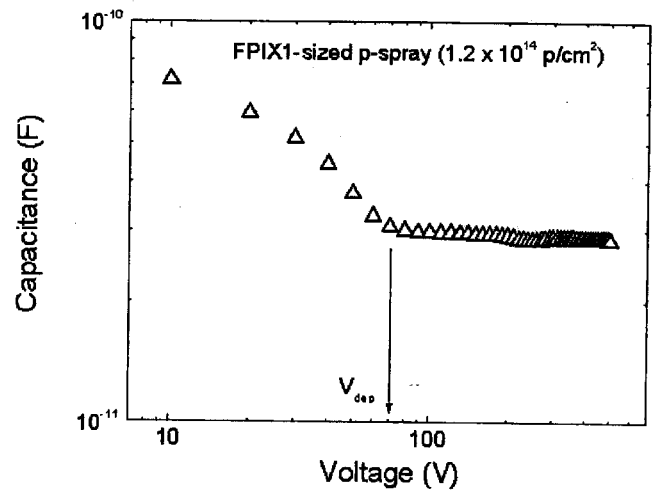


Fig. 9. Example of bulk capacitance versus bias potential measurement used to determine the depletion voltage of a p-spray FPIX1-sized sensor.

In order to estimate the depletion voltage C-V measurements were performed also for the p-spray sensors. Fig. 9 show the capacitance versus the bias voltage for the most irradiated sensor and we determine that the  $V_{\text{dep}} \sim 70$  V. For the sensor irradiated up to  $8 \times 10^{13}$  p/cm<sup>2</sup> we have  $V_{\text{dep}} \sim 45$  V. Before the irradiation, for these sensors we had  $V_{\text{dep}} \sim 60$  V. From a comparison of these results and the results obtained for the p-stop sensors at the same radiation dose, we see that, whereas for the p-stop sensors at  $1.2 \times 10^{14}$  p/cm<sup>2</sup> there is still no type inversion, for the p-spray sensors,

instead the type inversion already has occurred. This is due to the high resistivity of the p-spray sensors.

More tests are in progress in order to better investigate the performance of the p-spray isolation technique.

## VI. CONCLUSION

A first characterization of the prototype BTeV silicon pixel sensors is presented. Two different pixel isolation techniques were considered: p-stop and p-spray. For the SINTEF p-stop pixel sensors, experimental results based on I-V and C-V measurements are promising. Most of the tested sensors meet the specifications: leakage current less than 50 nA/cm<sup>2</sup> and breakdown voltage above 300 V. From the point of view of the radiation hardness with proton fluence, SINTEF low-resistivity sensors have excellent performance. However, we see that for this pixel layout there is the problem connected with the fact that not all the single cells can be easily and safely grounded simultaneously.

For the p-spray pixel sensors, the results are promising too, but more tests need to be done. In this case, there are no ground problems due to the fact that a bias grid structure can be implemented.

## VII. ACKNOWLEDGMENTS

We would like to thank to the ATLAS collaboration to provide us with p-spray sensors.

## VIII. REFERENCES

- [1] A. Kulyavtsev, M. Procario, J. Russ, J. You, J. Cumalat, J. Appel, et al. "BTeV proposal," Fermilab, May 2000.
- [2] E. E. Gottschalk, "BTeV detached vertex trigger," Fermilab-CONF-01-088-E, June 2001.
- [3] D. C. Christian, J. A. Appel, G. Cancelo, S. W. Kwan, J. Hoff, A. Mekkaoui, et al. "Development of a pixel read out chip for BTeV," *Nucl. Instr. Meth.*, A 335, 144 (1999).
- [4] G. Batagnani, F. Bosi, L. Bosisio, A. Conti, E. Focardi, F. Forti, et al., "Double-sided readout silicon strip detectors for the ALEPH minivertex," *Nucl. Instr. Meth.*, vol. A 277, pp 147-153, 1989.
- [5] R. H. Richter, L. Andricek, T. Gebhart, D. Hauff, J. Kemmer, G. Lutz, et al., "Strip detector design for ATLAS and HERA-B using two-dimensional device simulation," *Nucl. Instr. Meth.*, vol. A 377, pp 412-421, 1996.
- [6] G. Lutz, et al., Streifen-detektor, Patentoffenlegungsschrift-OS 196 20 081 A1 21.11.97, Munich, 1997.
- [7] R. H. Richter, et al., "Moderate p-spray-an n-side isolation technique for highly irradiated silicon detectors," *Nucl. Instr. Meth.*, submitted.
- [8] B. Bischoff, N. Findeis, D. Hauff, P. Holl, J. Kemmer, P. Klein, et al., "Breakdown protection and long-term stabilisation for Si-detectors," *Nucl. Instr. Meth.*, vol. A 326, pp 27-37, 1993.
- [9] ATLAS TDR 5, CERN/LHCC/97-17, ISBN 92-9083-103-0.
- [10] L. Evensen, A. Hanneborg, B. S. Avset, and M. Nese, "Guard ring design for high voltage operation of silicon detectors," *Nucl. Instr. Meth.*, vol. A 337, p 44-52, 1993.
- [11] R. Della Marina, CSEM Centre Suisse d'Electronique et Microtechnique SA (Switzerland), private communication, 1999.
- [12] N. Bacchetta, D. Bisello, A. Candelori, M. Da Rold, M. Descovich, A. Kaminski, et al., "Improvement in breakdown characteristics in the multiguard structures in microstrip silicon detectors for CMS," *Nucl. Instr. Meth.*, vol. A 461, p 204-206, 2001.
- [13] G.P. Summer, E.A. Burke, P. Shapiro, S.R. Messenger, and R.J. Walters, "Damage correlation in semiconductors exposed to gamma, electron, and proton irradiation," *IEEE Trans. Nucl. Sci.* vol. 40, p 1372, 1993.
- [14] Annual Book of ASTM Standard, "Standard practice for characterizing neutron energy fluence spectra in terms of an equivalent monoenergetic neutron fluence for radiation-hardness testing of electronics," E772-94 vol. 12.02.
- [15] M.R. Coluccia, J.A. Apple, G. Chiodini, D.C. Christian and S.W. Kwan, "Characterization of prototype BTeV silicon pixel sensors before and after irradiation," accepted for publication in *IEEE Trans. Nucl. Sci.* Aug 2002,
- [16] G. Lutz, "Semiconductor radiation detectors: device physics," Springer 1999.